

# Fractal energy spectrum of a polariton gas in a Fibonacci quasi-periodic potential

D. Tanese<sup>1</sup>, E. Gurevich<sup>2</sup>, F. Baboux<sup>1</sup>, T. Jacqmin<sup>1</sup>, A. Lemaître<sup>1</sup>,  
E. Galopin<sup>1</sup>, I. Sagnes<sup>1</sup>, A. Amo<sup>1</sup>, J. Bloch<sup>1</sup>, E. Akkermans<sup>2</sup>

<sup>1</sup>Laboratoire de Photonique et de Nanostructures,

LPN/CNRS, Route de Nozay, 91460 Marcoussis, France and

<sup>2</sup>Department of Physics, Technion Israel Institute of Technology, Haifa 32000, Israel

(Dated: August 15, 2018)

We report on the study of a polariton gas confined in a quasi-periodic one dimensional cavity, described by a Fibonacci sequence. Imaging the polariton modes both in real and reciprocal space, we observe features characteristic of their fractal energy spectrum such as the opening of mini-gaps obeying the gap labeling theorem and log-periodic oscillations of the integrated density of states. These observations are accurately reproduced solving an effective 1D Schrödinger equation, illustrating the potential of cavity polaritons as a quantum simulator in complex topological geometries.

PACS numbers: 71.36.+c, 78.55.Cr, 78.67.-n, 05.45.Df, 61.43.Hv, 71.23.Ft

Free quantum particles or waves propagating in a spatially varying potential present modifications of their spectral density, which depend on the symmetry of this potential. The richness of spectral distributions in constrained geometries has long been recognized. The case of a periodic potential described by means of the Bloch theorem is a significant example. The notion of spectral distribution has been deepened in the wake of quasi-crystals discovery and it led to a classification of energy spectra into absolutely continuous, pure point and singular continuous spectral distributions [1]. The latter class proved to be surprisingly rich and it encompasses a broad range of potentials, such as quasi-periodic potentials which have been thoroughly studied [2, 3].

An interesting quasi-periodic potential can be designed using a Fibonacci sequence. The corresponding singular continuous energy spectrum has a fractal structure of the Cantor set type [4–7], and it displays self-similarity *i.e.*, a symmetry under a discrete scaling transformation. Denoting  $\rho(\varepsilon)$  the relevant density of states (DOS) in  $\varepsilon$  (either energy or frequency), a *discrete scaling symmetry* about a particular value  $\varepsilon_u$  is expressed by the property

$$\mu(\varepsilon_u + \Delta\varepsilon) - \mu(\varepsilon_u) = \frac{\mu(\varepsilon_u + \beta\Delta\varepsilon) - \mu(\varepsilon_u)}{\alpha}, \quad (1)$$

where  $\mu(\varepsilon) = \int_{-\infty}^{\varepsilon} \rho(\varepsilon') d\varepsilon'$  is the integrated density of states (IDOS), or density measure, and  $\alpha$  and  $\beta$  are scaling parameters which usually, depend on  $\varepsilon_u$ . Defining a shifted IDOS by  $\mathcal{N}_{\varepsilon_u}(\varepsilon) \equiv \mu(\varepsilon) - \mu(\varepsilon_u)$ , the general solution of (1) can be written as [8]

$$\mathcal{N}_{\varepsilon_u}(\varepsilon) = |\varepsilon - \varepsilon_u|^\gamma \mathcal{F}\left(\frac{\ln|\varepsilon - \varepsilon_u|}{\ln\beta}\right), \quad (2)$$

where  $\gamma = \frac{\ln\alpha}{\ln\beta}$  is the local ( $\varepsilon_u$ -dependent) scaling exponent and  $\mathcal{F}(z)$  is a periodic function of period unity, whose (non-universal) form depends on the problem at hand. Generally, the exponent  $\gamma$  takes values between zero and unity, so that the density  $\rho(\varepsilon)$  is a singular function. Such scaling properties of a fractal spectrum are

expected to modify the behavior of physical quantities [8]. Recently studied examples include thermodynamic properties of photons [9], random walks [10], quantum diffusion of wave packets [11] and spontaneous emission triggered by a fractal vacuum [12]. The diffusion of a wave packet in a quasi-periodic medium is predicted to be neither diffusive, nor ballistic but to present a behavior characterized by non-universal exponents and a log-periodic modulation of its time dynamics. Experimental demonstration of these specific properties of quasi-periodic structures is still missing as yet. We propose to use cavity polaritons to evidence such a fractal behavior.

Cavity polaritons are quasi-particles arising from the strong coupling between the optical mode of an optical cavity and excitons confined in quantum wells [13]. They have appeared recently as a promising system to realize quantum simulators [14, 15]. Engineering of the potential landscape is possible and allows implementing a large variety of physical situations such as 1D [14, 16, 17] and 2D periodic potentials [18, 19] with the generation of gap solitons [17, 20], non-linear resonant tunneling devices [21], or triangular [22] and honeycomb [23, 24] lattices, which enables the exploration of graphene physics. Polaritons offer experimental possibilities not available in 1D or 2D photonic quasi-crystals such as direct time- and energy-resolved measurements of the excitations in both space and momentum domains. Thus, one can directly visualize individual eigenmodes, and the dynamics of wave packets.

In this letter, we use this well-controlled system to investigate both theoretically and experimentally the spectral properties of a polariton gas in a quasi-periodic potential. To do so, we have sculpted the lateral profile of a quasi-1D cavity in the shape of a Fibonacci sequence. Using non resonant excitation in the low density regime, we probe the modes both in real and reciprocal space. We observe a quantitative agreement between experiments and the calculated modes and density of states. In particular, we evidence features of a fractal energy spectrum,

namely gaps densely distributed and an integrated density of states (IDOS) reflecting the existence of a discrete scaling symmetry as expressed by (2).

In our sample, cavity polaritons are confined within narrow strips (wire cavities), whose width is modulated quasi-periodically. These wires are fabricated processing a planar high quality factor ( $Q \sim 72000$ ) microcavity grown by molecular beam epitaxy. It consists in a  $\lambda/2$   $Ga_{0.05}Al_{0.95}As$  layer surrounded by two  $Ga_{0.8}Al_{0.2}As/Ga_{0.05}Al_{0.95}As$  Bragg mirrors with 28 and 40 pairs in the top/bottom mirrors respectively. 12 GaAs quantum wells of width 7 nm are inserted in the structure resulting in a 15 meV Rabi splitting. 200  $\mu m$  long wires with lateral dimension modulated quasi-periodically are designed using electron beam lithography and dry etching (Figs. 1(a-b)). The modulation consists in two wire sections ("letters")  $A$  and  $B$  of same length  $a$  but different widths  $w_A$  and  $w_B$  respectively (Fig.1(b)). The modulation of the wire width induces an effective 1D potential for the longitudinal motion of polaritons, as discussed in the sequel. The letters are arranged according to the Fibonacci sequence [4] using the recursion,

$$S_{j \geq 3} = [S_{j-2}S_{j-1}], \text{ and } S_1 = B, S_2 = A, \quad (3)$$

where  $[S_{j-2}S_{j-1}]$  means concatenation of two subsequences  $S_{j-2}$  and  $S_{j-1}$ . The number of letters (length) of a sequence  $S_j$  is given by the Fibonacci number  $F_j$ , such that  $F_{j+1} = F_j + F_{j-1}$ . The ratio  $F_{j+1}/F_j$  tends to the golden mean  $\sigma = (1 + \sqrt{5})/2 \simeq 1.62$  in the limit  $j \rightarrow \infty$ , while the corresponding sequence  $S_\infty$  becomes rigorously quasi-periodic and invariant, *i.e.* self-similar, under the iteration transformation (3). Our sample corresponds to  $S_{13}$  counting 233 letters with  $a = 0.8 \mu m$ ,  $w_A = 3.5 \mu m$  and  $w_B = 1.86 \mu m$ . To study the po-

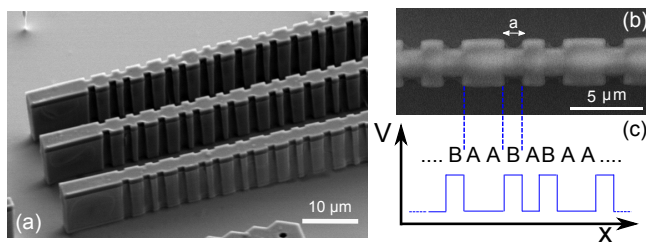


FIG. 1: (Color online) (a) Scanning electron microscopy image of an array of modulated wires. (b) Zoom on a particular wire, showing the shape of the A and B letters. (c) Schematic of the nominal potential corresponding to the lateral shaping of the wire cavity.

lariton modes in these quasi-periodic wires, we perform low temperature (10 K) micro-photoluminescence experiments. Single wires are excited non-resonantly using a cw monomode laser tuned typically 100 meV above the polariton resonances. The excitation spot extends over a 80  $\mu m$ -long region along the wire. The sample emis-

sion is collected with a 0.65 numerical aperture objective and focused on the entrance slit (parallel to the wire) of a spectrometer coupled to a CCD camera. Imaging of the sample surface (resp. the Fourier plane of the collection objective) allows studying the spectrally resolved polariton modes in real (resp. reciprocal) space. Excitation power is kept low enough to stay below condensation threshold and obtain a nearly homogeneous population of the lower energy polariton states.

Fig.2.a displays the spatially and spectrally resolved emission measured on a single modulated wire cavity for an exciton-photon detuning around  $-8 meV$  (defined as the energy difference between the cavity mode at normal incidence and the exciton resonance). Several polariton modes are imaged. They present complex patterns of bright spots distributed all over the region of the wire under investigation. To understand the nature of these modes and properties of their spectral density, we have calculated the polariton eigenstates in such quasi-periodic structures.

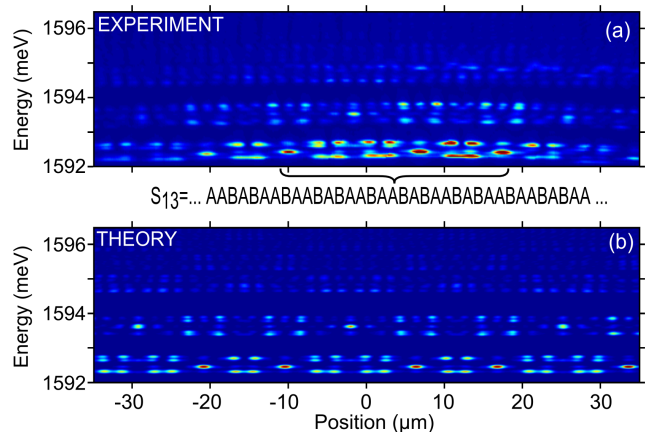


FIG. 2: (Color online) (a) Spectrally and spatially resolved emission measured on a single modulated wire (the linear polarization parallel to the wire is selected). Bottom of the figure: letter sequence corresponding to a part of the whole  $S_{13}$  potential sequence. (b) Calculated polariton Fibonacci modes as a function of energy and real space coordinate.

In our model whose details are given in the supplement [25], we describe the confined photon modes using a 2D scalar wave equation with vanishing boundary conditions on the boundary of the wire, considered as an axially symmetric strip where the longitudinal coordinate  $x \in [0, L]$  ( $L$  being the length of the wire), and the transverse coordinate  $-\frac{w(x)}{2} \leq y \leq \frac{w(x)}{2}$ . Here,  $w(x) > 0$  accounts for the  $x$ -dependent width of the wire (Fig.1.c), *i.e.* a quasi-periodic sequence of segments of width  $w_A$  and  $w_B$ , as defined in (3). In the supplement [25], we show how to map this 2D problem onto a 1D Schrödinger equation

with the effective potential:

$$V(x) = \frac{\pi^2}{w^2(x)} + \frac{\pi^2 + 3}{12} \left( \frac{w'(x)}{w(x)} \right)^2. \quad (4)$$

The first term of  $V(x)$  is the usual adiabatic approximation. The second term accounts for the sharpness of the steps. It is not perturbative, and it cannot be neglected (see supplement [25]). As clearly visible on Fig.1, the strip shape is not perfectly abrupt but presents some smoothness in the width variation introduced by the actual etching process. The smoothness scale is used as a fitting parameter in the calculations. The eigenfunctions  $\phi_q(x)$  and eigenenergies  $E_{C,q}$  are obtained numerically. To calculate the polariton modes, we consider the radiative coupling between excitons with a flat dispersion to the photon modes we have obtained in our simulations. Since the coupling is diagonal in the index  $q$ , the resulting polariton eigenfunctions and photons have the same spatial behavior. Fig. 2.b shows the polariton modes thus obtained numerically. Since experimentally we cannot resolve states which are separated by less than the polariton linewidth, we have averaged the intensity over eigenmodes close in energy. Thus, what appears in Fig.2.b as bright intensity spots at different energies are actually bands separated by gaps. Clearly the calculation reproduces very accurately the spatial structure of the polariton modes observed in the experiment. This direct imaging of the Fibonacci modes in a quasi-periodic structure is a clear asset offered by cavity polaritons.

Probing the polariton modes in reciprocal space provides also remarkable information about the eigenmodes. This is illustrated on Fig.3.a, where taking advantage of the one-to-one relation between angle of emission and in-plane momentum of polaritons, far field imaging of the polariton emission is shown for the same wire as in Fig.2. A complex band structure appears with the opening of gaps not regularly spaced unlike the case of a periodic modulation [17]. The calculated band structure reproduces quantitatively the measurements (Fig.3.b).

In the rest of the paper, we show that despite the finite size of the system, both in the numerics and in the experiments, fundamental physical properties are evidenced in this complex band-structure which indicate the onset of a fractal density of states. To study the spectrum and the position of its gaps, it is convenient to rewrite the quasi-periodic potential  $V(x)$  in (4) under the form,

$$V(x) = \sum_n \chi(\sigma^{-1}n) u_b(x - an) \quad (5)$$

valid in principle [4] for an infinitely long system namely  $j \rightarrow \infty$  in (3).  $u_b(x)$  (which depends on  $w(x)$ ) describes the shape of the letter  $B$  while the periodic function  $\chi(x)$  defined, within  $[0, 1]$ , by  $\chi(x) = 1$  for  $0 < x < 2 - \sigma$  and  $\chi(x) = 0$  for  $2 - \sigma < x < 1$ , accounts for the quasi-periodic order. The Fourier transform of  $V(x)$  consists

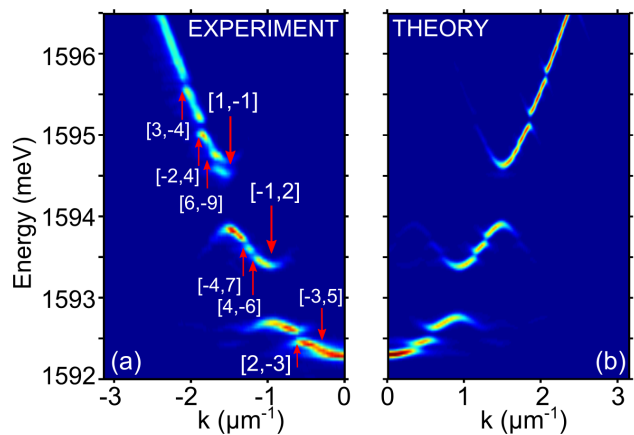


FIG. 3: (Color online) (a) Spectrally resolved far field emission measured on the same wire cavity used in Fig.2; (b) Corresponding simulation. Position of the gaps labeled with two integers  $[p, q]$  is indicated with red arrows.

of Bragg peaks and is given by,

$$V(k) = \tilde{u}_b(k) \sum_{p,q} \chi_q \delta(k a - 2\pi(p + q\sigma^{-1})) \quad (6)$$

with obvious notations. Since  $\sigma$  is irrational, each Bragg peak of the quasi-periodic potential can be uniquely labeled with a set  $[p, q]$  of two integers so that the corresponding wave number is  $k = Q_{p,q} \equiv \frac{2\pi}{a} (p + q\sigma^{-1})$ . Similarly to the Bloch theorem for a periodic modulation, we may expect that a series of gaps opens at each independent Bragg peak  $Q_{p,q}$ . Thus, to label the gaps and to obtain the IDOS given in (2), it is tempting to consider the quasi-periodic potential  $V(x)$  as a small perturbation. Albeit not justified in the present experimental case, we shall first use this assumption since it allows to give a more intuitive derivation of gap labeling. But the Bragg peaks being a dense set, we must be cautious and first approximate  $\sigma$  by its finite approximants  $\sigma_j = F_{j+1}/F_j$  as defined after (3). Then,  $V(x)$  in (5) becomes a periodic approximant  $V_{j+1}(x)$ , built from periodically repeated cells  $S_{j+1}$  of length  $a F_{j+1}$ . Thus, the properties of the single cell  $S_{j+1}$  studied experimentally are essentially those of the periodic potential  $V_{j+1}(x)$ . Its Fourier transform  $V_{j+1}(k)$  is obtained replacing  $\sigma$  by  $\sigma_j$  in (6).  $V_{j+1}(k)$  thus defined, is the structure factor of a periodic structure and therefore it has a finite density of Bragg peaks spaced by  $\Delta k = 2\pi/(aF_{j+1})$ . Perturbation theory in  $|V| \ll 1$  is now applicable. To first order, each Bragg peak  $k = Q_{p,q} \equiv \frac{2\pi}{a} (F_{j+1}p + F_j q)$  hybridizes the degenerate Bloch waves at wave numbers  $\pm Q_{p,q}/2$ . The coupling between these plane waves is best described by a two-level Hamiltonian with diagonal,  $\varepsilon \equiv E_{Q_{p,q}/2} = E_{-Q_{p,q}/2}$ , and off-diagonal,  $V_q \equiv V_{\chi_q}$ , matrix elements. The doubly degenerate level  $\varepsilon$  splits into  $\varepsilon \pm |V_q|$  and a gap of width  $2|V_q|$  opens at this en-

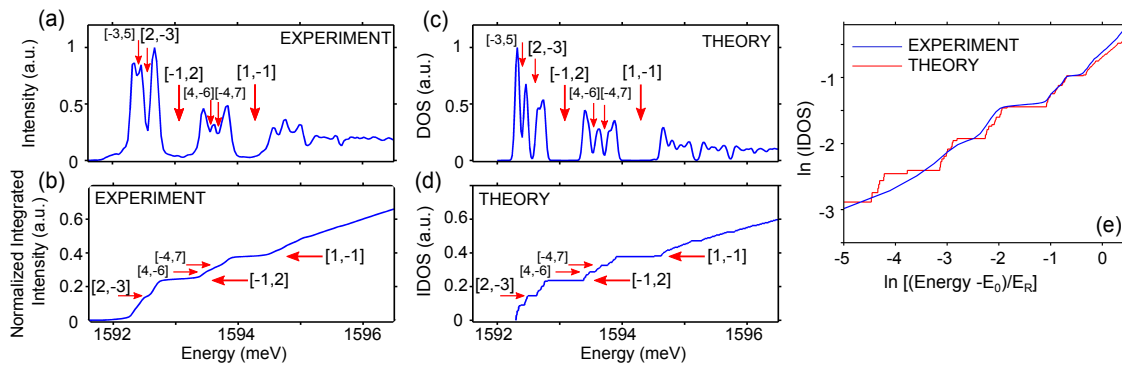


FIG. 4: (Color online) (a) Measured total (angularly integrated) emission spectrum  $I(\varepsilon)$  of the quasi-periodic wire and (b) Spectrally integrated emission intensity  $\int_{E_0}^{\varepsilon} I(\varepsilon') d\varepsilon'$  (where  $E_0$  is the lower energy state); (c-d) Calculated normalized DOS (c) and IDOS (d). (e) Display of the log-periodic oscillations of the IDOS in a log-log plot of numerical (red) and experimental (blue) IDOS in the vicinity of  $E_0$  (normalized to  $E_R = \hbar^2 \pi^2 / (8a^2 m_p)$ , with  $m_p$  the polariton mass).

ergy. Accordingly, there is a one-to-one correspondence between the Bragg peaks and the gaps generated through the hybridization of plane waves, so that each gap can also be labeled with the two integers  $[p, q]$ . Noting that  $Q_{p,q} a/2\pi = p + q\sigma^{-1}$  is the proportion of unperturbed eigenmodes whose energies are less than  $\varepsilon = E_{Q_{p,q}/2}$ , the IDOS inside the  $[p, q]$ -gap is

$$\mathcal{N}(\varepsilon = E_{Q_{p,q}/2}) = p + q\sigma^{-1} = q\sigma^{-1} \pmod{1} \quad (7)$$

for  $\mathcal{N}(\varepsilon = E_{Q_{p,q}/2})$  normalized to unity at  $E_{Q_{1,0}}$ .

While the previous result has been obtained using perturbation theory, it happens that it has a much broader range of validity generally expressed by the so called gap labeling theorem [27] formulated by Bellissard and coworkers. This theorem provides a precise framework for applicability and allows to compute values of the IDOS in the gaps of the spectrum of 1D Schrödinger Hamiltonians with bounded potentials  $V(x)$ . An important consequence of that theorem is the topologically stable nature of the IDOS values in the gaps which extends beyond perturbation theory. Those specific values are obtained [27] from some prescribed linear combinations of components of eigenvectors of the corresponding substitution matrix characteristic of the quasi-periodic potential. For the Fibonacci sequence defined in (3), that prescription reduces to linear combinations of 1 and  $\sigma^{-1}$  namely to (7). In Fig.3.a, we indicate with red arrows the labeling of the gaps using the set  $[p, q]$ , demonstrating that the positions of the gaps are accurately determined by the positions of the Bragg peaks even for a relatively short Fibonacci sequence such as considered here. These positions are topological quantities, namely independent of the strength of the potential. These observed spectral features are thus independent of the (large enough) sample size and of the realization of the potential. These points are further discussed in the supplement [25]. On the other hand, the energy width of the gaps depends on

the heights of the Bragg peaks, *i.e.* on the details of the potential  $u_b(x)$  (and  $w(x)$ ).

The peculiar structure of the emission spectrum appears also clearly by considering the total emission intensity  $I(\varepsilon)$  nearly proportional to the DOS for low excitation powers. Fig.4.a displays peaks and deeps corresponding respectively to bands and pseudo-gaps. The measured integrated intensity  $\int_{E_0}^{\varepsilon} I(\varepsilon') d\varepsilon'$  (with  $E_0$  being the lower energy state), is reported in Fig.4.b together with the numerically calculated DOS and IDOS (Figs 4.c-d). Applying (7), valid in principle in the infinite limit, to the gaps  $[2, -3]$ ,  $[-1, 2]$ ,  $[1, -1]$  indicated in Figs.4.b-d, gives respectively  $\mathcal{N}(E_{Q_{p,q}/2}) = 0.15, 0.24, 0.38$ . These numbers are in excellent agreement with the experiment, confirming the good homogeneity achieved in populating the polariton states.

For the infinite system, there exists an infinite series of gaps at  $p + q\sigma^{-1} \in [0, 1]$ . Thus the energy spectrum, which is the complementary of these gaps, is singular continuous. It is a Cantor like set whose total width vanishes. The high resolution available in the numerics allows to consider finer details of the IDOS as predicted by the scaling form (2). In Fig.4.e, we have plotted in a log-log scale the IDOS as a function of (properly normalized) energy. It is noticeable that, even for such a finite sized system, we indeed observe a power law behavior multiplied by a log-periodic function. More interesting is the experimental observation of these log-periodic oscillations, showing two periods of oscillations, which constitutes a direct and so far unobserved signature of the fractal character of the Fibonacci spectrum.

In summary, probing the luminescence of a polariton gas laterally confined by a Fibonacci quasi-periodic potential, we have observed the characteristic behavior of the associated fractal energy spectrum: gaps densely distributed, and an IDOS well described by the scaling form (2) and following the gap labeling theorem (7). We have

obtained a spectrally and spatially resolved image of the polariton modes which is in good quantitative agreement with theoretical and numerical results. Our results support the idea that topological features of a fractal spectrum are robust and show up quite accurately even for a relatively short structure. Those results evidence the great interest of cavity polaritons to study the anomalous time expansion of a polariton wave-packet [11], more complex quantum systems *e.g.* 2D quasi-crystals [28] and more generally to realize quantum simulators.

**Acknowledgements:** This work was supported by the Israel Science Foundation Grant No.924/09, by the 'Agence Nationale pour la Recherche' project "Quandyde" (ANR-11-BS10-001), by the FP7 ITN "Clermont4" (235114), by the french RENATECH network, the LABEX NanoSaclay and the Honeywell ERC starting grant.

- 
- [1] H.L. Cycon, R.G. Froese, W. Kirsch and B. Simon, *Schrödinger Operators*, (Springer, Berlin, 1987) and M. Reed and B. Simon, *Methods of Modern Mathematical Physics* (Academic Press, California, 1980).
- [2] D. Damanik and A. Gorodetski, *Commun. Math. Phys.* **305**, 221 (2011) and D. Damanik, M. Embree, A. Gorodetski, S. Tcheremchantsev, *Commun. Math. Phys.* **280**, 499 (2008)
- [3] For a recent review see Z. V. Vardeny, A. Nahat and A. Agrawal, *Nature Photonics* **7**, 177187 (2013).
- [4] M. Kohmoto, B. Sutherland and C. Tang, *Phys. Rev. B* **35**, 1020 (1987); J.M. Luck, *Phys. Rev. B* **39**, 5834 (1989).
- [5] W. Gellermann, M. Kohmoto, B. Sutherland and P.C. Taylor, *Phys. Rev. Lett.* **72**, 633 (1994).
- [6] M. Kohmoto, L.P. Kadanoff and C. Tang, *Phys. Rev. Lett.* **50**, 1870 (1983) and S. Ostlund and S.Kim, *Physica Scripta* **9**, 193 (1985). For a review see E.L. Albuquerque and M.G. Cottam, *Phys. Rep.* **376**, 225 (2003); E. Maciá, *Rep. Prog. Phys.* **69**, 397 (2006).
- [7] M. Kohmoto, B. Sutherland and K. Iguchi, *Phys. Rev. Lett.* **58**, 2436 (1987); D. Würtz, T. Schneider and M.P. Soerensen, *Physica A* **148**, 343 (1988).
- [8] For a recent review, E. Akkermans, *Contemporary Mathematics* **601**, 1-22 (2013), arXiv:1210.6763.
- [9] E. Akkermans, G.V. Dunne and A. Teplyaev, *Phys. Rev. Lett.* **105**, 230407 (2010).
- [10] E. Akkermans, O. Benichou, G. Dunne, A. Teplyaev and R. Voituriez, *Phys. Rev. E* **86**, 061125 (2012).
- [11] I. Guarneri and G. Mantica, *Phys. Rev. Lett.* **73**, 3379 (1994) and S. Abe and H. Hiramoto, *Phys. Rev. A* **36**, 5349 (1987).
- [12] E. Akkermans and E. Gurevich, *Europhys. Lett.* **103**, 30009 (2013).
- [13] C. Weisbuch, M. Nishioka, A. Ishikawa, and Y. Arakawa, *Phys. Rev. Lett.* **69**, 3314 (1992)
- [14] C. W. Lai, N. Y. Kim, S. Utsunomiya, G. Roumpos, H. Deng, M. D. Fraser, T. Byrnes, P. Recher, N. Kumada, T. Fujisawa and Y. Yamamoto, *Nature* **450**, 529 (2007)
- [15] I. Carusotto and C. Ciuti, *Rev. Mod. Phys.* **85**, 299 (2013)
- [16] E. A. Cerda-Méndez, D. N. Krizhanovskii, M. Wouters, R. Bradley, K. Biermann, K. Guda, R. Hey, P. V. Santos, D. Sarkar, and M. S. Skolnick, *Physical Review Letters* **105**, 116402 (2010)
- [17] D. Tanese, H. Flayac, D. Solnyshkov, A. Amo, A. Lemaître, E. Galopin, R. Braive, P. Senellart, I. Sagnes, G. Malpuech and J. Bloch, *Nature Communication* **4**, 1749 (2013)
- [18] N. Y. Kim, K. Kusudo, C. Wu, N. Masumoto, A. Löffler, S. Höfling, N. Kumada, L. Worschech, A. Forchel and Y. Yamamoto, *Nature Physics* **7**, 681 (2011)
- [19] E. A. Cerda-Méndez, D. N. Krizhanovskii, K. Biermann, R. Hey, M. S. Skolnick, and P. V. Santos, *Phys. Rev. B* **86**, 100301 (2012).
- [20] E. A. Cerda-Méndez, D. Sarkar, D. N. Krizhanovskii, S. S. Gavrilov, K. Biermann, M. S. Skolnick, and P. V. Santos, *Phys. Rev. Lett.* **111**, 146401 (2013)
- [21] H. S. Nguyen, D. Vishnevsky, C. Sturm, D. Tanese, D. Solnyshkov, E. Galopin, A. Lemaître, I. Sagnes, A. Amo, G. Malpuech, and J. Bloch *Phys. Rev. Lett.* **110**, 236601 (2013)
- [22] N. Y. Kim, K. Kusudo, A. Löffler, S. Höfling, A. Forchel, and Y. Yamamoto, *New Journal of Physics* **15**, 035032 (2013)
- [23] N. Y. Kim, A. Löffler, S. Höfling, A. Forchel, and Y. Yamamoto, *Phys. Rev. B* **87**, 214503 (2013)
- [24] T. Jacqmin, I. Carusotto, I. Sagnes, M. Abbarchi, D. Solnyshkov, G. Malpuech, E. Galopin, A. Lemaître, J. Bloch and A. Amo, arXiv:1310.8105 (2013).
- [25] See supplementary materials.
- [26] L. D. Negro, C. J. Oton, Z. Gaburro, L. Pavesi, P. Johnson, A. Lagendijk, R. Righini, M. Colocci, and D. S. Wiersma, *Phys. Rev. Lett.* **90**, 055501 (2003).
- [27] J. Bellissard, A. Bovier and J.M. Ghez, *Reviews in Math. Physics*, Vol. 4, No. 1, 1-37 (1992) and B. Simon, *Adv. Appl. Math.* **3**, 463 (1982) and J. Bellissard, *Les Houches*, Springer, J.M. Luck, P. Moussa and M. Waldschmidt Eds., (1993).
- [28] J-M. Gambaudo and P. Vignolo, arXiv:1309.6420 (2013).

# Supplementary material for "Fractal energy spectrum of a polariton gas in a Fibonacci quasi-periodic potential"

D. Tanese<sup>1</sup>, E. Gurevich<sup>2</sup>, F. Baboux<sup>1</sup>, T. Jacqmin<sup>1</sup>, A. Lemaître<sup>1</sup>,  
E. Galopin<sup>1</sup>, I. Sagnes<sup>1</sup>, A. Amo<sup>1</sup>, J. Bloch<sup>1</sup>, E. Akkermans<sup>2</sup>

<sup>1</sup>*Laboratoire de Photonique et de Nanostructures,  
LPN/CNRS, Route de Nozay, 91460 Marcoussis, France and*

<sup>2</sup>*Department of Physics, Technion Israel Institute of Technology, Haifa 32000, Israel*  
(Dated: February 24, 2014)

In this Supplementary Material, we present additional experimental data supporting our claim about fractal properties of the Fibonacci spectrum and in particular the invariance of the IDOS in the gaps in accordance with the gap labeling theorem (7) discussed in the Letter. We then present a brief but explicit derivation of the 1D Schrödinger equation with the effective potential  $V(x)$  given by equation (4) of the Letter. We stress the importance of the second, often omitted, term in  $V(x)$  and then compare the results obtained within this effective 1D approach to those obtained using a full fledged numerical calculation of the 2D polariton spectrum.

## EXPERIMENTAL ILLUSTRATION OF THE TOPOLOGICAL INVARIANCE OF THE IDOS

In order to illustrate the topological invariance of the integrated density of states (IDOS) measured on a polariton gas laterally confined by a Fibonacci potential, we describe here additional data obtained for different system sizes and realizations of the potential. The results are presented in a similar way as in the paper so that they can be directly compared to Figs. 3 and 4. These new data confirm that the wave vector values at which the mini-gaps open in the Fibonacci spectrum, as well as the corresponding values of the IDOS, are invariant quantities of topological nature, *i.e.* that they do not depend on the specific shape of the quasi-periodic potential felt by the polaritons nor on the size of the letters.

We study two additional samples (hereafter called samples 2 and 3 by contrast to sample 1 which corresponds to the one presented in the Letter). These samples have a different length  $a$  of the letters than sample 1 (which had  $a = 0.8 \mu\text{m}$ ). Sample 2 has longer letters ( $a = 1.35 \mu\text{m}$ ), while sample 3 has shorter ones ( $a = 0.5 \mu\text{m}$ ). Furthermore, while sample 3 has letter widths identical to those of sample 1 ( $w_A = 3.5 \mu\text{m}$  and  $w_B = 1.86 \mu\text{m}$ ), sample 2 has a different  $w_B = 2.04 \mu\text{m}$ , which results in a smaller potential contrast between the two types of letters. Moreover samples 2 and 3 also differ from sample 1 by their total number of letters, and thus correspond to different orders of the Fibonacci sequence:  $S_{12}$  (144 letters) for sample 2,  $S_{14}$  (377 letters) for sample 3, as compared to  $S_{13}$  (233 letters) for sample 1.

Figures 1 and 2 display the spectrally resolved far field emission, the density of states (DOS) and the IDOS measured on samples 2 and 3, together with corresponding calculations.

Let us first discuss the far field emission shown in the top panels of the two figures. As in Fig. 3 of the Letter, mini-gaps open, whose positions in momentum space can be accurately labeled (see arrows) by means of two inte-

gers  $[p, q]$  such that  $k = \frac{\pi}{a}(p + q\sigma^{-1})$ , in accordance with the gap labeling theorem (7). Comparing these spectra with sample 1 allows to understand their scaling properties. Since the momentum  $k$ -positions of the gaps scale as  $\frac{\pi}{a}$ , the spectrum of sample 2 appears "compressed" in energy with respect to that of sample 1: for instance, the gap  $[-1, 2]$  appears much closer to the bottom of the parabola. Thus, due to the finite polariton linewidth, only one mode is visible below this gap (instead of three for sample 1 in the Letter). For sample 3 instead, the spectrum appears "stretched" with respect to sample 1, and more modes and mini-gaps can be experimentally identified below this  $[-1, 2]$  gap than in the Letter.

The values of the IDOS in the mini-gaps are also invariant topological quantities. This is illustrated in Figs. 1(d) and 2(d) where the theoretical values  $\mathcal{N}(E_{Q_{p,q}/2}) = p + q\sigma^{-1}$  for the IDOS inside the gaps (see Eq. (7) of the Letter), predicted by the gap labeling theorem, are indicated with red horizontal arrows. Both numerical and experimental results reproduce well the values of the heights of the plateaus.

To conclude, the overall data presented in our work provides a solid illustration of the scaling properties of the gaps positions and topological invariance of the IDOS, as ensured by the gap labeling theorem (7).

## DERIVATION OF THE EXPRESSION OF THE EFFECTIVE POTENTIAL GIVEN BY EQUATION (4)

We now turn to the derivation and discussion of the validity of the 1D Schrödinger equation with the effective potential  $V(x)$ ,

$$V(x) = \frac{\pi^2}{w^2(x)} + \frac{\pi^2 + 3}{12} \left( \frac{w'(x)}{w(x)} \right)^2 \quad (1)$$

given by Eq. (4) in the Letter. To that aim, we need to map the original 3D setup onto an effective 1D prob-

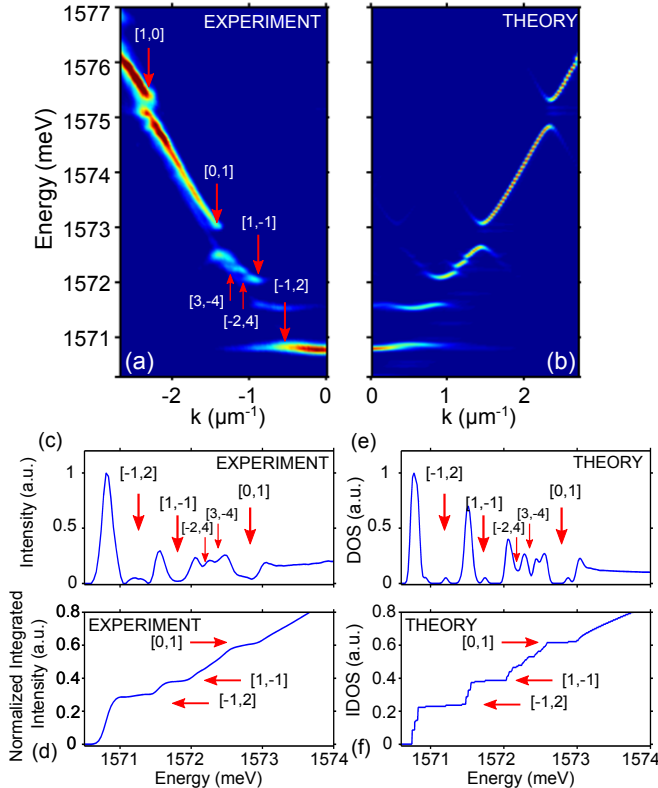


FIG. 1: (Color online) (a) Spectrally resolved far field emission measured on sample 2 (parameters given in the text) and (b) corresponding numerical results obtained with the effective 1D model described in the Letter and in the next section. The positions of the gaps are labeled with two integers  $[p, q]$  and indicated with red arrows. (c) Measured total (angular-averaged) emission spectrum  $I(\varepsilon)$  and (d) normalized integrated emission intensity  $\int_{E_0}^{\varepsilon} I(\varepsilon') d\varepsilon'$  (with  $E_0$  the lower energy state). (e) Calculated DOS smoothed for the comparison with  $I(\varepsilon)$  in (c). (f) Normalized calculated IDOS.

lem. As described in more detail in the Letter, polaritonic wires are fabricated by processing a planar  $\lambda/2$  cavity. We denote  $n$  its effective refractive index. The electromagnetic field is confined along the (vertical)  $z$ -direction using two Bragg mirrors. This confinement is much tighter than that in the perpendicular  $xy$ -plane. For the latter, we impose zero boundary conditions, an approximation justified by the high contrast in refractive index between dielectric and air (see, e.g., Ref. [1]). Under the above assumptions, the corresponding electromagnetic field eigenmodes can be chosen to have either TE or TM polarizations. The polarization splitting is large in an etched wire cavity, probably because of strain relaxation. Since in the experiment we detect only one polarization, we do not include the polarization degree of freedom in the simulation and we consider a scalar wave approximation. Then, looking for separable solutions between vertical and lateral coordinates, leads to the follow-

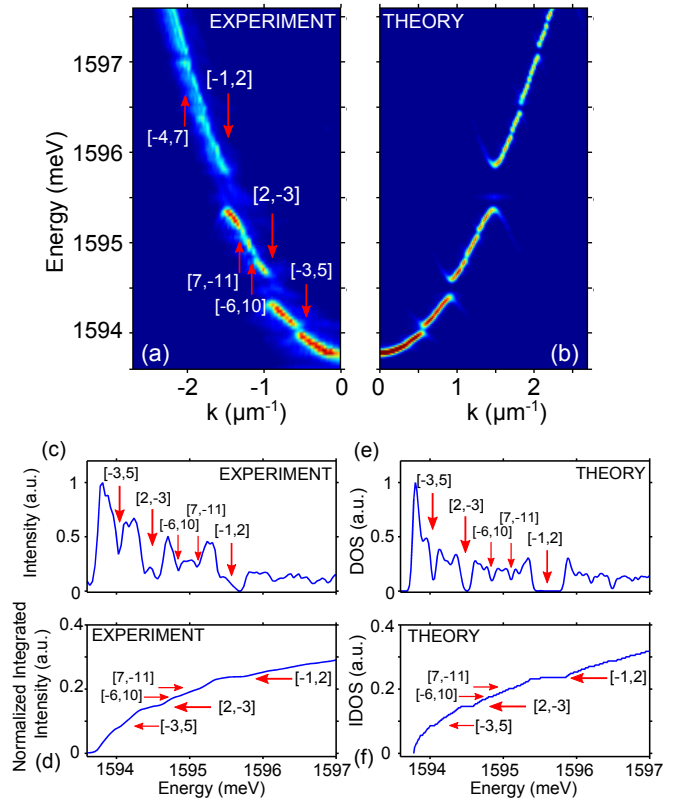


FIG. 2: (Color online) Same as Fig. 1 for sample 3 (parameters in the text).

ing two-dimensional (2D) stationary wave equation

$$E\psi(x, y) = -\frac{\hbar^2}{2m_{ph}} \Delta_{\perp} \psi(x, y), \quad (2)$$

where  $m_{ph} \equiv n^2 E_c / c^2$  is the effective photon mass,  $E_c \equiv \frac{\hbar c}{n} k_z$  is the energy associated with the fundamental mode of the  $\lambda/2$  cavity, and  $\Delta_{\perp} \equiv \partial_x^2 + \partial_y^2$  is the transverse Laplacian. Since  $E \ll E_c$ , the total photon energy can be expanded in  $E$  so that,

$$\hbar\omega \approx E_c + E. \quad (3)$$

As a result of our assumed zero boundary conditions in the  $xy$ -plane, the electromagnetic field  $\psi(x, y)$  vanishes on the boundary.

Note that Eq.(2), with the same boundary conditions, also holds to describe the center-of-mass motion of the excitons confined to the  $xy$ -plane by the quantum wells. Therefore, within the same approximations, the electromagnetic field and the excitons have similar eigenmodes and energy spectrum (up to the difference in their effective mass), so that the photon-exciton coupling is diagonal in the eigenmode index. A flat exciton dispersion is used because of their relatively large mass. The finding of the eigenmodes of the 2D problem (2) on a strip can easily be done numerically. Nevertheless, it is useful to have

a well controlled 1D effective model providing intuition and insight of the essential features of the problem at hand. This is particularly relevant for the quasi-periodic potential we study and its fractal polariton spectrum, since a broad range of analytical and numerical tools are specifically available for the 1D problem, such as the gap labeling theorem used in the Letter.

To proceed further and establish the expression of the 1D effective potential Eq.(1), we look for solutions of the wave equation Eq. (2) on a symmetric strip defined by its longitudinal coordinate  $x \in [0, L]$ , where  $L$  is the length of the wire, and its transverse coordinate  $-\frac{w(x)}{2} \leq y \leq \frac{w(x)}{2}$ . The function  $w(x) > 0$ , which defines the  $x$ -dependent width of the wire, is assumed to be differentiable. The sought solution can generally be written in the form of a Fourier series over the transverse quasi-modes,

$$\psi(x, y) = \sum_{n=0}^{\infty} \psi_n(x) \sqrt{\frac{2}{w(x)}} \cos(k_{y,n}(x)y), \quad (4)$$

where both the transverse wave vector,  $k_{y,n}(x) = \pi \frac{2n+1}{w(x)}$ , and the expansion coefficients  $\psi_n(x)$ , are  $x$ -dependent. This solution is symmetric with respect to the middle line  $y = 0$ , and it is not coupled to the similar anti-symmetric one (note that for a non-symmetric strip, both solutions would participate to the expansion (4)). We need to consider only symmetric solutions, since they include the lowest frequency branch, corresponding to the lowest transverse quasi-mode,  $k_{y,0}(x) = \frac{\pi}{w(x)}$ . An infinite hierarchy of coupled differential equations for  $\psi_m(x)$  is obtained by substituting the expansion (4) into the wave equation (2) and subsequently integrating over  $y$  with the weight  $\sqrt{\frac{2}{w(x)}} \cos(k_{y,m}(x)y)$ . Neglecting the coupling to the higher quasi-modes, leads to the following approximate equation for the lowest quasi-mode:

$$E\psi_0(x) = \frac{\hbar^2}{2m_{ph}} \left[ -\frac{d^2}{dx^2} + V(x) \right] \psi_0(x), \quad (5)$$

where  $V(x)$  given in Eq.(1), defines the effective 1D potential along the strip for the lowest transverse mode. Similar results have been obtained for the study of cold atoms in optical trap waveguides [2]. The coupling of  $\psi_0(x)$  to the higher quasi-modes leads to the appearance of additional terms in Eq.(5), involving various derivatives of  $w(x)$ . For a coupling strength between quasi-modes small compared to the energy separation to the next mode, we can neglect those additional terms. The detailed analysis of this conditions is, however, beyond the scope of this supplement. Instead, we justify this approximation comparing our results to the full fledged 2D numerics.

The first term in the potential  $V(x)$  given in Eq.(1) is the usual adiabatic approximation, proportional to

$k_{y,0}^2(x)$ , which accounts for the distribution of the "kinetic" energy between the transversal and the longitudinal degrees of freedom. For a constant  $w(x)$ , the problem is separable. It leads to uncoupled transverse modes  $\psi_m(x)$  and the adiabatic kinetic term is the only remaining contribution to  $V(x)$ . For a varying profile  $w(x)$  such as the one we consider, the problem is not separable anymore, and the second term in Eq.(1) becomes relevant. This term is sensitive to the stiffness of the boundary variation [2]. For a smoothly varying width,  $w'(x)$  is small and the second term is negligible compared to the kinetic term. For a sharper step structure, like the one we consider (see Fig. 1(b)-(c) of the Letter), the two terms in the effective potential become comparable. In the limit in of sharp steps for  $V(x)$ , the second term in Eq.(1) becomes singular, namely a repulsive  $\delta$ -function squared. In that case, higher transversal quasi-modes must be included.

### COMPARISON BETWEEN THE EXACT 2D CALCULATION AND THE EFFECTIVE 1D POTENTIAL

We wish now to show that the effective 1D model provides a quantitatively good description of the measured polariton spectrum provided we include the second term in the potential (1) which account for the sharp boundary modulation. To that purpose, we compare the low energy eigenmode spectra obtained from the exact two-dimensional (2D) and the effective one-dimensional calculations. The 2D calculation is done using, instead of (4), a complete two-dimensional Fourier expansion, and then diagonalizing the Hamiltonian in this two-dimensional basis. In addition, a scale is introduced over which we smoothen the width profile by means of a convolution of the binary width profile with the Gaussian kernel,

$$g(x) \propto e^{-(x/\eta a)^2}, \quad (6)$$

where  $a$  is the letter length and the relative dimensionless smoothness scale  $\eta$  is used as a fitting parameter (to the experimental data). This is justified looking at the micrograph of the wire in Fig. 1(b) of the Letter. Obviously, there is some smoothness in the wire width variation, introduced by the etching process. Its scale, however, is hard to quantify from the direct measurement, and should be considered as a phenomenological parameter. In order to compare the effective 1D description to the full 2D calculation, we consider sample 2 described above ( $a = 1.35 \mu\text{m}$ ), and plot in Fig. 3 the integrated density of states (IDOS) for different values of the fitting parameter  $\eta$ . We note that the position and the width of the gaps of the 2D spectrum are significantly less sensitive to the parameter  $\eta$  than the effective 1D spectrum. Note



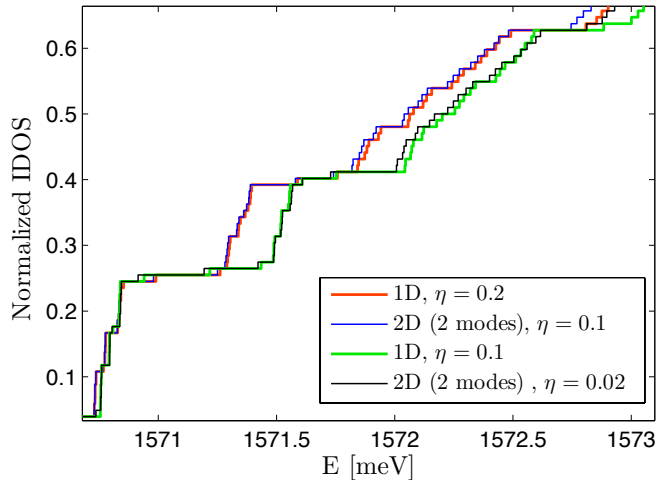


FIG. 3: (Color online) Comparison, for sample 2, between the results obtained for the IDOS based on the full 2D and the 1D calculations using the effective potential  $V(x)$  given by Eq. (1). The values of smoothing parameter  $\eta$  are indicated in the inset.

however, that the value of the IDOS in the gaps is independent of  $\eta$  in both cases, since it is a topologically stable quantity. These different sensitivities to the parameter  $\eta$  can be rather exactly compensated by increasing the smoothness scale in the 1D calculation relatively to the corresponding 2D case. This is demonstrated in

Fig. 3 by superimposing the two results for different sets of choices of  $\eta$ . On the other hand, the 1D calculation using only the first (kinetic) term in  $V(x)$  does not show any specific dependence on  $\eta$  even for rather large values of the smoothing. It is thus not possible to use this approximation to reproduce the 2D calculation. Moreover, the 1D potential based on the first kinetic term only in Eq.(1), is unable to reproduce the gap structure of the spectrum, even qualitatively. To show this, we have plotted in the left panel of Fig. 4, the spectral function of the 2D calculation. It is compared (right panel) to the 1D spectral function obtained using the first term only in Eq. (1). We note the discrepancy in the position of the gaps which cannot be handled by a proper choice of  $\eta$ . More important, the higher energy gaps (*e.g.* the one labeled  $[1, 0]$ ) in Fig. 3 of the Letter are missing. In contrast, the full 1D effective model with a proper value of  $\eta$  reproduces faithfully both the 2D and the measured spectra.

- 
- [1] A. Kuther, M. Bayer, T. Gutbrod, A. Forchel, P. A. Knipp, T. L. Reinecke, and R. Werner, Phys. Rev. B **58**, 15744 (1998).
  - [2] S Schwartz, M Cozzini, C Menotti, I Carusotto, P Bouyer and S Stringari, New Journal of Physics **8**, 162 (2006).

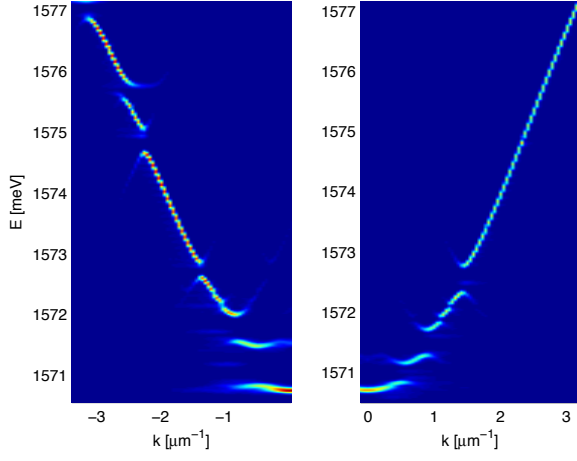


FIG. 4: (Color online) Comparison, for sample 2, between the spectral function obtained from the full 2D calculation (left) versus the 1D calculation using the effective potential  $V(x)$  given by Eq.(1) where only the first kinetic term has been considered (right).